

## ON THE CORRELATION BETWEEN CO ABSORPTION AND FAR-ULTRAVIOLET NON-LINEAR EXTINCTION TOWARD GALACTIC OB STARS

ERIC B. BURGH, STEPHAN R. MCCANDLISS, B-G ANDERSSON, AND PAUL D. FELDMAN  
 Department of Physics and Astronomy, The Johns Hopkins University, Baltimore, MD 21218

*To appear in the Astrophysical Journal, September 20, 2000*

### ABSTRACT

A sample of 59 sight lines to reddened Galactic OB stars was examined for correlations of the strength of the CO Fourth Positive ( $A^1\Pi - X^1\Sigma^+$ ) absorption band system with the ultraviolet interstellar extinction curve parameters. We used archival high-dispersion NEWSIPS IUE spectra to measure the CO absorption for comparison to parametric fits of the extinction curves from the literature. A strong correlation with the non-linear far-UV curvature term was found with greater absorption, normalized to  $E(B - V)$ , being associated with more curvature. A weaker trend with the linear extinction term was also found. Mechanisms for enhancing CO in dust environments exhibiting high non-linear curvature are discussed.

*Subject headings:* Dust, extinction — ISM: abundances — ISM: molecules — ultraviolet: ISM

### 1. INTRODUCTION

The extinction of starlight in the ultraviolet (UV;  $\lambda \lesssim 3200 \text{ \AA}$ ) can be characterized by three main components: a linear rise, a Lorentzian-like bump centered on  $\lambda \sim 2175 \text{ \AA}$ , and a far-ultraviolet ( $\lambda \lesssim 1700 \text{ \AA}$ ) non-linear rise. The general features of the extinction curve can be understood in terms of dust grain populations (Mathis, Rumpl, & Nordsieck 1977; Draine & Lee 1984, e.g.). Cardelli, Clayton, & Mathis (1988, 1989) showed that the overall shape of the UV extinction curve can be estimated by the single parameter  $R_V[\equiv A(V)/E(B - V)]$ . However, individual sight lines exhibit large deviations from the average extinction curve, particularly in the far-UV rise (Mathis & Cardelli 1992). A detailed understanding of these deviations can provide information about the nature of the particles responsible for the extinction, putting constraints on interstellar grain models.

A number of studies have investigated the possible correlations between the various components of the UV extinction curve and gas phase abundances (Joseph et al. 1989; Jenniskens et al. 1992), infrared emissions (Cox & Leene 1987; Hackwell et al. 1991; Boulanger, Prevot, & Gry 1994), very broadband structure (Jenniskens 1994), and diffuse interstellar band (DIB) absorptions (Désert, Jenniskens, & Deneffeld 1995). The Jenniskens et al. (1992) study was the first to positively identify a correlation of the strength of the non-linear rise with the abundance of a gas phase atom or molecule, finding that a larger column of CH implies a stronger far-UV non-linear rise, and the inverse relationship for CH<sup>+</sup>.

No such study has to date been performed for CO, a molecule of great astrophysical importance. Being the second most abundant molecule after H<sub>2</sub>, it is used as a tracer of H<sub>2</sub> gas and an indicator of the total mass of molecular clouds (Scoville et al. 1987; Bloemen 1989; Hunter et al. 1994). Having allowed rotational transitions that are readily observed in emission at radio wavelengths, the CO molecule is commonly used to probe dark molecular clouds. CO also has an extensive band system in the ultraviolet, which can be used to investigate the molecular

content of diffuse and translucent clouds when observed in absorption toward background stars.

The wavelength coverage of the short-wavelength prime (SWP) camera of the *International Ultraviolet Explorer* (IUE) satellite, 1150 – 2000 Å, spans as many as 19 bands of the Fourth Positive ( $A^1\Pi - X^1\Sigma^+$ ) ( $v'-0$ ) band system beginning with the (0–0) band at 1544.5 Å and continuing to shorter wavelengths. For this study, we searched the IUE archival data for ultraviolet absorption of CO along 59 lines of sight toward Galactic O and B stars for which UV extinction curves have already been published, and parameterized as described below, to investigate the possible correlations with the various curve features.

Fitzpatrick & Massa (1990, FM hereafter) have proposed a parameterization that accurately fits the extinction curves with a single analytical expression using six parameters. Using this method, the extinction curve, normalized to unit  $E(B - V)$  and with  $x \equiv \lambda^{-1}$ , can be expressed as

$$k(x) \equiv \frac{E(\lambda - V)}{E(B - V)} = c_1 + c_2x + c_3D(x; \gamma, x_0) + c_4F(x) \quad (1)$$

where

$$D(x; \gamma, x_0) = \frac{x^2}{(x^2 - x_0^2)^2 + x^2\gamma^2} \quad (2)$$

is the Lorentzian-like “Drude” profile, representing the 2175 Å bump with  $x_0$  the bump peak and  $\gamma$  its width, and

$$F(x) = \begin{cases} 0.53(x - 5.9)^2 + 0.05446(x - 5.9)^3 & x > 5.9\mu\text{m}^{-1} \\ 0 & x \leq 5.9\mu\text{m}^{-1} \end{cases} \quad (3)$$

is the far-UV curvature term, whose strength is determined by a single parameter,  $c_4$ .

### 2. THE SAMPLE

Our sample consists of 59 reddened stars ( $0.24 \leq E(B - V) \leq 1.09$ ). The UV extinction curves for these stars have been previously determined using the pair method by FM and Aiello et al. (1988). The extinction curve parameters for stars from the Aiello et al. sample are taken from Jenniskens & Greenberg (1993, JG hereafter), who used the

FM fitting routine. For stars that appear in both samples, we adopt the FM numbers. The parameters from JG show a small ( $1\text{-}\sigma$ ) systematic offset from the FM data, producing slightly smaller  $c_2$  values and larger  $c_4$  values, approximately  $-0.1$  and  $+0.1$  respectively. These systematic errors do not significantly affect the results of the analysis.

Of the stars in the FM and JG samples, only those for which high-dispersion short-wavelength IUE spectra exist are considered here. We also consider only stars of spectral type B5 and earlier and luminosity classes III and V, since spectral mismatch using the pair method can strongly affect the extinction curve fitting at later types and higher luminosities (Massa et al. 1983). Although these stars do not represent a purely random sampling of interstellar sight lines, they do sample different interstellar environments, including dense and diffuse media, as well as regions of recent early-type star formation.

### 3. ANALYSIS

For each star high-dispersion short-wavelength New Spectral Image Processing System (NEWSIPS) IUE spectra were obtained from the archive maintained by the Astrophysics Data Facility (ADF). The quality of the data varies strongly from object to object due to the differences in exposure time, brightness of the source, and number of spectra available. To improve the signal-to-noise per source, multiple spectra were co-added by weighted mean when available. However, no further processing was performed on the data. Figure 1 shows examples of both strong and weak CO absorption.

We measured the equivalent width of the (2–0) band in each spectrum. A linear continuum was fit and the equivalent width measured by integrating over the absorption line profile (typically a span of  $0.4\text{--}1\text{ \AA}$ ). The  $1\text{-}\sigma$  error was computed by summing the normalized errors for each pixel in quadrature. For non-detections, the upper limit was taken to be the error computed across  $0.4\text{ \AA}$ . The measured equivalent widths and the IUE exposure numbers for each star are listed in Table 1.

The (2–0) band, located near  $1477.6\text{ \AA}$ , was chosen for several reasons. It is well separated from the nearby  $^{13}\text{CO}$  band at  $1478.8\text{ \AA}$  and is relatively uncontaminated by other interstellar or stellar features for all the spectral types considered in this study. It is also the least susceptible to background subtraction errors known to occur in NEWSIPS data because it lies near the sensitivity peak of the echelle spectrograph (Massa et al. 1998). It also has the highest band oscillator strength of the Fourth Positive band system and thus is the most likely to be observed in low  $S/N$  data.

The resolution of the IUE echelle spectrograph ( $R \approx 10^4$ ) combined with the limiting  $S/N$  ( $\approx 20 : 1$ ) of the SEC vidicon detectors (Cowie & Songaila 1986) conspires to restrict our typical  $2\text{-}\sigma$  equivalent width detection limit to  $\approx 30\text{ m\AA}$ . As we will show in the Appendix, even at this equivalent width, all absorption lines are affected by saturation and thus the conversion of the molecular band equivalent width to a corresponding column density depends on assumptions of the gas rotational excitation temperature,  $T$ , and doppler velocity,  $b$ . Although the various sight lines are likely to have different values for  $T$  and  $b$ , on average the values for these parameters lie around  $T \approx 4$

K and  $b \approx 1\text{ km s}^{-1}$  (Gredel, van Dishoeck, & Black 1991), as observed in higher quality data. We will adopt these values to convert the equivalent width to column density for the comparison to previous work and allow a statistical assessment of the robustness of our result with respect to the phenomenologically more meaningful column density.

For sight lines whose CO absorption has been previously studied our measurements agree very well with the published data. In particular, the equivalent widths for the (2–0) bands of HD 21483, HD 47129, and HD 149757 of  $322 \pm 27$  (Joseph et al. 1986),  $46 \pm 17$  (Tarafdar & Krishna Swamy 1982), and  $74 \pm 7$  (Wannier et al. 1982) all agree within the error with our measured values. Four more sight lines (HD 34078, HD 37903, HD 147933, and HD 193322) have been observed in other bands, either higher  $A - X$  bands or the shorter wavelength  $B - X$  and  $C - X$  bands. Column densities for all of these stars are compiled in Federman et al. (1994). By converting our measured equivalent width to column density as described in the Appendix we directly compare our results for all the aforementioned sight lines in Figure 2.

For the purpose of comparison to the extinction curve parameters as specified in Equation 1, the equivalent width is normalized to unit reddening. This produces a measure of the relative abundance of CO to the total amount of matter along the line of sight. Figure 3 shows the correlation plots of this quantity versus each of the six extinction curve parameters for the stars listed in Table 1.

These data were analyzed using the Astronomy SURVival Analysis (ASURV) software package Rev 1.2 (Isobe & Feigelson 1990; LaValley, Isobe, & Feigelson 1992), which implements the survival analysis methods presented in Feigelson & Nelson (1985) and incorporates the upper limits in a statistically appropriate manner. For each parameter of the extinction curve, the Spearman's Rho value, a non-parametric rank-order correlation coefficient, was computed. This value, which can range between 1 and  $-1$  for a perfect correlation and anti-correlation respectively, was tested for its significance by calculating a  $t$ -value, which is distributed approximately as Student's distribution with  $N - 2$  degrees of freedom and is effectively a measure of the standard deviations from the null hypothesis. This allows the probability that the correlation could be drawn randomly from this distribution to be determined. These results are tabulated in Table 2.

### 4. RESULTS AND DISCUSSION

No significant correlations were seen with the extinction curve parameters  $x_0$ ,  $\gamma$ , or  $c_3$  (see Figure 3). The relationship with  $c_2$  (middle right panel of Figure 3), while not showing a linear correlation does show an interesting bifurcation. (FM note that  $c_1$  and  $c_2$  are strongly correlated and thus only the relationship with  $c_2$  is considered here.) Although a high  $c_2$  does not guarantee a large CO abundance, the largest abundances are seen when  $c_2 > 0.5$ . Of notable exception is HD 147889. This highly reddened star ( $E(B - V) = 1.09$ ) has a  $c_2$  of 0.151 but the absorption suggests a column density as high as  $3 \times 10^{17}\text{ cm}^{-2}$ . However, it must be noted that this star has a high  $c_4$  value of 0.709. As  $c_2$  is inversely proportional to  $R_V$  (Fitzpatrick 1999), our result would suggest that lower CO abundances would be observed along sight lines with

$R_V \gtrsim 3.6$ . Cardelli (1988) noted a decline in the abundances of  $\text{H}_2$  and  $\text{CH}$  with increasing  $R_V$  and a similar break in the  $\text{CH}$  abundance at  $R_V = 3.5$  for clouds with  $A_V < 2$ . The interstellar average  $R_V$  is 3.1, which corresponds to a  $c_2$  of 0.7, and thus it is apparent that the slope of the linear rise is not the dominant factor determining the abundance of  $\text{CO}$  in average clouds.

The plot with  $c_4$ , the strength of the non-linear far-UV rise, (left panel of Figure 4 – same as bottom right panel of Figure 3) shows the  $\text{CO}$  abundance being correlated with stronger far-UV curvature. We note that for  $c_4 \gtrsim 0.5$  we always detect  $\text{CO}$  and only upper limits exist for  $c_4$  below 0.25. This suggests that the carrier of the non-linear rise has a more direct association with the  $\text{CO}$  abundance than that of the linear rise ( $c_2$ ). The right panel of Figure 4 shows the relationship between the  $\text{CO}$  column density per  $E(B - V)$  and  $c_4$  assuming  $b = 1 \text{ km s}^{-1}$  and  $T = 4 \text{ K}$ . Although these values are likely not correct for each individual star it demonstrates the effective range of column densities observed and the lower limit of detectability by IUE. This correlation produces a Spearman's Rho of 0.630, consistent with the equivalent width relationship.

The abundance of  $\text{CO}$  along a given sight line is governed by the balance between formation through chemical networks involving species such as  $\text{C}^+$ ,  $\text{OH}$ , and  $\text{CH}$ , and destruction through photodissociation (van Dishoeck & Black 1988; Federman & Huntress 1989). The correlation of  $\text{CO}$  with  $c_4$  suggests that the presence of the carrier of the non-linear far-UV extinction is conducive to the presence of  $\text{CO}$ . This can be accomplished either by not destroying  $\text{CO}$  through shielding of the photodissociating flux or by aiding in the formation of  $\text{CO}$  by not photodissociating the precursor molecules.

$\text{CO}$  photodissociates through the discrete absorptions of far-UV photons resulting in the excitation of the molecule into predissociating states. At the edges of clouds, this occurs primarily through the  $E - X$  (0-0) band at 1076 Å. However, as optical depth increases into the cloud, most of the photodissociation moves to shorter wavelength transitions (van Dishoeck & Black 1988), where the extinction of flux by the non-linear rise increases dramatically. van Dishoeck & Black (1989) have demonstrated that the photodissociation rate of  $\text{CO}$  is reduced in cloud models that use steeper extinction curves to model the continuum extinction of far-UV flux. It is therefore possible that we are observing an increase in molecular content associated with a decrease in photodestruction since the strength of the parameters  $c_2$  and  $c_4$  regulate the far-UV flux at short wavelengths. This is suggested in Figure 5, where we show the relation of these parameters to the  $\text{CO}$  normalized equivalent width. However, it is important to realize that the actual attenuation of radiation in a cloud depends strongly on the far-UV scattering characteristics of the grains responsible for the extinction, even when the extinction rises sharply in the far-UV (Flannery et al. 1980).

Although Figure 5 is suggestive, it is far from conclusive. If the carrier of the non-linear rise aids in the formation of  $\text{CO}$ , or any of its precursor molecules, such as  $\text{CH}$  and  $\text{OH}$ , the  $\text{CO}$  formation rate may be enhanced enough to explain the rapid increase in column densities seen in Figure 4.

## 5. CONCLUSIONS

The abundance of  $\text{CO}$ , as measured by the equivalent width of the UV absorption of the  $A - X$  (2-0) band normalized to unit  $E(B - V)$ , is correlated with the strength of the non-linear far-UV rise in the UV extinction curves toward Galactic O and B stars. This correlation is indicative of either a decrease in the photodestruction rate of  $\text{CO}$  with increased extinction or of a dust environment that is conducive to the enhanced formation of  $\text{CO}$  or its precursor molecules. The linear rise does not correlate with  $\text{CO}$  abundance, although for sight lines with large  $R_V$  ( $\gtrsim 3.6$ ) we observe mostly small columns ( $\lesssim 10^{15} \text{ cm}^{-2}$  per  $E(B - V)$ ). These results, together with those of Cardelli (1988) reinforces the notion that the use of the visual extinction,  $A_V$ , as the independent variable in global studies of interstellar chemistry has to be viewed with some caution.

Future study of these relationships could benefit from a quantitative determination of the  $\text{CO}$  column density and an exploration of the  $\text{H}_2/\text{CO}$  ratio in these environments. For  $\text{H}_2$ , the ideal instrument is the recently launched *Far-Ultraviolet Spectroscopic Explorer* (FUSE) satellite. FUSE will be able to measure the  $\text{H}_2$  column from the individual lines of the Werner and Lyman band systems, as well as observe the absorptions from the  $\text{CO}$  Hopfield-Birge bands. However, more accurate  $\text{CO}$  observations could be made by the Space Telescope Imaging Spectrograph (STIS) for two reasons. The wavelength separation of the rotational lines within the  $A - X$  bands is greater than that of the  $B - X$  and  $C - X$  and the STIS Echelle modes have higher resolution than FUSE, allowing for the measurement of the ground state rotational temperature and doppler velocity, and therefore a precise derivation of column density. Finally, we note that the ratio of true absorption to scattering by dust in the far-UV is critical to the interpretation of these results. Studies aimed at investigating this relation in conjunction with the FM extinction parameterization would be useful. Such measurements would facilitate a more detailed analysis of the conditions in these cloud environments.

All IUE data were obtained from the Astrophysics Data Facility at NASA's Goddard Space Flight Center. The authors would like to thank Derck Massa for valuable discussions. We also thank the referee, Steve Federman, for several helpful comments and suggestions. This work was supported by NASA grant NAG5-5122 to The Johns Hopkins University.

## APPENDIX

Typically, the column density is derived from the measured equivalent width through the use of an appropriate curve-of-growth. For molecules, the shape of a band integrated curve-of-growth depends strongly on the rotational excitation temperature,  $T$ , of the molecules and the line-broadening doppler parameter,  $b$ . Unfortunately, the spectral resolution of the IUE data is not high enough to allow for a direct measurement of the  $b$  parameter and only in the cases of the

strongest absorptions is it possible to put limits on the rotational temperature from the observed absorption profile.

The use of multiple bands could produce a more accurate column density determination by limiting the possible values of  $b$  and  $T$ . However, to fit the relative amounts of absorption in multiple bands with a single model based on three parameters ( $N$ ,  $b$ , and  $T$ ) it is desirable to have accurate equivalent widths of more than three bands. The (0–0) and (1–0) bands of the  $A - X$  band system have blended  $^{12}\text{CO}$  and  $^{13}\text{CO}$  components. The (3–0) and (4–0) bands can sometimes be measured although the continuum has definite structure for some of the spectral types of stars considered in this study, while the (5–0) band is blended with the Si IV  $\lambda 1394$  feature. Thus, the measurement of the equivalent width of these bands is dependent on an accurate fit to the continuum in these regions. The (6–0) band is not usually blended with other features, but it has an oscillator strength five times weaker than the (2–0) band and is only observed for the largest column density sight lines. Figure 6 shows band integrated curves-of-growth for the (2–0), (3–0), and (4–0) bands of the CO  $A - X$  band system computed using the band oscillator strengths and line wavelengths of Morton & Noreau (1994). The (4–0) band is blended with the  $a' - X$  (14–0) band due to quantum mechanical mixing of these states. All of these bands show the effects of saturation above the IUE detection limit. As can be appreciated from the following example, attempts to fit the equivalent widths of multiple bands can produce non-unique solutions to  $N$ ,  $b$ , and  $T$ . A typical measurement (HD 192281 e.g.) yields  $W_{(2-0)} = 140 \pm 13 \text{ m}\text{\AA}$ ,  $W_{(3-0)} = 130 \pm 16 \text{ m}\text{\AA}$ , and  $W_{(4-0)} = 94 \pm 13 \text{ m}\text{\AA}$ . Utilizing the curves-of-growth shown in Figure 6 we find that within the range of reasonable  $b$ -values and rotational excitation temperatures the uncertainty in column density is approximately two orders of magnitude.

Another approach is to synthesize a model spectrum that can be compared directly to the data. We attempted to solve for  $N$ ,  $b$ , and  $T$  by generating a grid of models with various values for these parameters and minimizing the  $\chi^2$  value determined. This method proved successful only for those sight lines with the highest column density ( $\sim 10^{17} - 10^{18} \text{ cm}^{-2}$ ). The column density derived this way was usually within a factor of 2 or 3 of the value determined by assuming  $T = 4 \text{ K}$  and  $b = 1 \text{ km s}^{-1}$ . However, for smaller column sight lines ( $\sim 10^{16} \text{ cm}^{-2}$ ) the column derived differed by as much as an order of magnitude. This is due to the fact that the absorption profiles for these columns at the resolution of IUE strongly mix the effects of differing  $T$  and  $b$ , especially at low  $T$ . These results suggest that the assumption of average values for  $T$  and  $b$  may be justified for a statistical comparison to the extinction curve parameters, but may not produce reliable answers on an individual basis.

#### REFERENCES

- Aiello, S., Barsella, B., Chlewicki, G., Greenberg, J. M., Patriarchi, P., & Perinotto, M. 1988, *A&AS*, 73, 195  
 Bloemen, H. 1989, *ARA&A*, 27, 469  
 Boulanger, F., Prevot, M. L., & Gry, C. 1994, *A&A*, 284, 956  
 Cardelli, J. A. 1988, *ApJ*, 335, 177  
 Cardelli, J. A., Clayton, G. C., & Mathis, J. S. 1988, *ApJ*, 329, L33  
 Cardelli, J. A., Clayton, G. C., & Mathis, J. S. 1989, *ApJ*, 345, 245  
 Cowie, L. & Songaila, A. 1986, *ARA&A*, 24, 499  
 Cox, P., & Leene, A. 1987, *A&A*, 174, 203  
 Désert, F. X., Boulanger, F., & Puget, J. L. 1990, *A&A*, 237, 215  
 Désert, F. X., Jenniskens, P., & Dennefeld, M. 1995, *A&A*, 303, 223  
 Draine, B. T., & Lee, H. M. 1984, *ApJ*, 285, 89  
 Dwek, E., et al. 1997, *ApJ*, 475, 565  
 Federman, S. R. & Huntress, W. T., Jr. 1989, *ApJ*, 338, 140  
 Federman, S. R., Strom, C. J., Lambert, D. L., Cardelli, J. A., Smith, V. V., & Joseph, C. L. 1994, *ApJ*, 424, 772  
 Feigelson, E. D., & Nelson, P. I. 1985, *ApJ*, 293, 192  
 Fitzpatrick, E. L. 1999, *PASP*, 111, 63  
 Fitzpatrick, E. L., & Massa, D. 1990, *ApJS*, 72, 163  
 Flannery, B. P., Roberge, W., & Rybicki, G. B. 1980, *ApJ*, 236, 598  
 Gredel, R., van Dishoeck, E. F. & Black, J. H. 1991, *A&A*, 251, 625  
 Hackwell, J. A., Hecht, J. H., & Tapia, M. 1991, *ApJ*, 375, 163  
 Hunter, S. D., Digel, S. W., De Geus, E. J., & Kanbach, G. 1994, *ApJ*, 436, 216  
 Isobe, T., & Feigelson, E. D. 1990, *BAAS*, 22, 917  
 Jenniskens, P. 1994, *A&A*, 284, 227  
 Jenniskens, P., Ehrenfreund, P., & Désert, F. X. 1992, *A&A*, 265, L1  
 Jenniskens, P., & Greenberg, J. M. 1993, *A&A*, 274, 439  
 Joblin, C., Léger, A., & Martin, P. 1992, *ApJ*, 393, L79  
 Joseph, C. L., Snow, T. P., Jr., Seab, C. G., & Crutcher, R. M. 1986, *ApJ*, 309, 771  
 Joseph, C. L., Snow, J., T. P., & Seab, C. G. 1989, *ApJ*, 340, 314  
 LaValley, M., Isobe, T., & Feigelson, E. D. 1992, *ASP Conf. Ser.* 25: *Astronomical Data Analysis Software and Systems I*, 1, 245  
 Massa, D., Savage, B. D., & Fitzpatrick, E. L. 1983, *ApJ*, 266, 662  
 Massa, D., Van Steenberg, M. E., Oliverson, N., & Lawton, P. 1998, in "Ultraviolet Astrophysics Beyond the IUE Final Archive", eds. Wamsteker and Riestra, *ESA SP-413*, p723.  
 Mathis, J. S., Rimpl, W., & Nordsieck, K. H. 1977, *ApJ*, 217, 425  
 Mathis, J. S., & Cardelli, J. A. 1992, *ApJ*, 398, 610  
 Morton, D. C., & Noreau, L. 1994, *ApJS*, 95, 301  
 Scoville, N. Z., Yun, M. S., Sanders, D. B., Clemens, D. P., & Waller, W. H. 1987, *ApJS*, 63, 821  
 Siebenmorgen, R., & Kruegel, E. 1992, *A&A*, 259, 614  
 Tarafdar, S. P., & Krishna Swamy, K. S. 1982, *MNRAS*, 200, 431  
 van Dishoeck, E. F., & Black, J. H. 1988, *ApJ*, 334, 771  
 van Dishoeck, E. F., & Black, J. H. 1989, *ApJ*, 340, 273  
 Verstraete, L., & Léger, A. 1992, *A&A*, 266, 513  
 Wannier, P. G., Penzias, A. A., & Jenkins, E. B. 1982, *ApJ*, 254, 100

TABLE 1  
STELLAR EXTINCTION CURVE AND CO ABSORPTION INFORMATION

Star	Sp. Type	$E(B - V)$	$c_2$	$c_4$	$W_{\text{CO}}(2-0)^a$ (mÅ)	Ref.	SWP number(s) <sup>b</sup>
HD 13268	O8V	0.44	1.03	0.38	$32 \pm 23$	1	09323
HD 14434	O6V	0.48	0.80	0.48	$< 67$	1	16094
HD 14442	O6III	0.73	0.69	0.44	$< 160$	1	53141
HD 15558	O5III	0.83	0.59	0.44	$106 \pm 40$	1	08322s
HD 15629	O5V	0.75	0.63	0.43	$135 \pm 25$	1	10754
HD 21483	B3III	0.55	0.730	0.658	$316 \pm 37$	2	38298
HD 34078	O9.5V	0.53	0.571	0.520	$< 126$	2	22108, 37429
HD 36629	B2V	0.27	0.21	0.31	$< 42$	1	10583
HD 36879	O8III	0.50	0.62	0.28	$34 \pm 13$	1	02711s, 04654s, 04699s
HD 36982	B2V	0.34	0.050	0.311	$< 36$	2	13733, 21973
HD 37022	O6p	0.34	0.033	0.186	$< 16$	2	07481, 13737, 13798, 14597, 15799, 19606
HD 37023	B0.5V	0.37	-0.083	0.153	$< 33$	2	02770, 05017s
HD 37061	B0.5V	0.54	0.109	0.044	$< 27$	2	07038, 08086
HD 37903	B1.5V	0.35	0.384	0.440	$< 23$	2	06953, 08058, 21293, 29094
HD 38087	B5V	0.33	0.230	0.311	$< 24$	2	30046, 32748, 32749, 32750
HD 46056	O8V	0.51	0.857	0.541	$148 \pm 37$	2	08846s
HD 46106	B0V	0.45	0.591	0.485	$55 \pm 23$	2	16435
HD 46149	O8.5V	0.48	0.65	0.59	$94 \pm 28$	1	21585, 28200
HD 46150	O6V	0.45	0.65	0.59	$127 \pm 19$	1	18947, 18948, 21584
HD 46202	O9V	0.47	0.864	0.515	$146 \pm 32$	2	30299
HD 46223	O4V	0.54	0.70	0.60	$107 \pm 15$	1	08138s, 08338s, 08844s, 10757
HD 47129	O8III	0.36	0.95	0.46	$38 \pm 10$	1	10689, 13924
HD 48099	O7V	0.27	0.874	0.339	$< 20$	2	52812, 52826, 52874
HD 48279	O8V	0.43	0.72	0.47	$60 \pm 20$	1	06504s
HD 48434	B0III	0.28	1.10	0.52	$< 46$	1	06447s
HD 73882	O8.5V	0.72	0.788	0.540	$246 \pm 18$	2	30076, 30077, 38299, 38311
HD 91824	O7V	0.27	0.633	0.473	$< 87$	2	16533
HD 93028	O9V	0.24	0.811	0.166	$< 69$	2	05521
HD 93204	O5V	0.43	0.48	0.37	$< 32$	1	07023, 07960
HD 93205	O3V	0.37	0.45	0.50	$< 28$	1	09635s, 09655s, 09672s, 09738s
HD 93222	O7III	0.40	0.626	0.236	$< 76$	2	22105
HD 93250	O3V	0.47	0.58	0.50	$70 \pm 20$	1	01618s, 06435s, 14746s
HD 93403	O5III	0.53	0.61	0.47	$92 \pm 17$	1	09075s, 09673s, 09739s
HD 96715	O4V	0.41	0.67	0.79	$198 \pm 19$	1	22000, 43980, 43981
HD 147888	B3V	0.52	0.133	0.339	$38 \pm 13$	2	05159s, 05160s
HD 147889	B2V	1.09	0.151	0.709	$221 \pm 40$	2	03924
HD 147933	B2V	0.47	0.139	0.349	$79 \pm 10$	2	25428, 25429, 25430, 25431, 25439
HD 149757	O9.5V	0.32	0.900	0.563	$81 \pm 8$	2	36152, 36155, 36162, 36164, 36167, 38410, 41190
HD 152233	O6III	0.45	0.74	0.45	$93 \pm 14$	1	40981, 40987, 40988
HD 154445	B1V	0.42	0.309	0.503	$< 44$	2	06760s
HD 162978	O8III	0.35	0.56	0.17	$< 15$	1	36945, 36948, 36949, 38302, 38303
HD 164816	B0V	0.30	0.37	0.35	$< 25$	1	02814s, 15308
HD 165052	O7V	0.43	0.39	0.28	$< 18$	1	15306, 17106, 45466, 45502
HD 167771	O7III	0.44	0.574	0.453	$62 \pm 13$	2	09623s, 09633s
HD 168076	O4V	0.80	0.48	0.46	$127 \pm 24$	1	28277
HD 192281	O5V	0.70	0.77	0.43	$140 \pm 13$	1	43147, 44636, 44637, 46539
HD 193322	O9V	0.41	0.879	0.115	$< 15$	2	31326, 31327, 31328, 31329, 36935, 36936
HD 199579	O6V	0.37	0.898	0.453	$139 \pm 13$	2	31317, 31318, 31323, 31331
HD 200775	B2V	0.54	0.54	0.52	$276 \pm 23$	1	09836, 09837, 54089
HD 215835	O6V	0.65	0.84	0.57	$54 \pm 34$	1	45467, 45503
HD 216532	O8V	0.86	0.53	0.40	$171 \pm 31$	1	34226
HD 216898	O8.5V	0.85	0.567	0.333	$169 \pm 34$	2	43934

TABLE 1—*Continued*

Star	Sp. Type	$E(B - V)$	$c_2$	$c_4$	$W_{\text{CO}}(2-0)^{\text{a}}$ (mÅ)	Ref.	SWP number(s) <sup>b</sup>
HD 217979	B2V	0.61	0.781	0.580	$297 \pm 92$	2	43935
HD 242908	O4V	0.60	0.54	0.45	$< 58$	1	16092
HD 303067	B0.5V	0.31	0.733	0.147	$< 63$	2	23759
HD 303308	O3V	0.45	0.55	0.43	$55 \pm 22$	1	09015s
BD +60 594	O9V	0.66	0.819	0.411	$103 \pm 67$	2	16644
BD +60 2522	B1V	0.72	0.66	0.41	$< 114$	1	08840
CPD -59 2600	O6V	0.53	0.601	0.179	$< 48$	2	07021

<sup>a</sup>errors are  $1 \sigma$ , upper limits are  $2\text{-}\sigma$

<sup>b</sup>an “s” indicates small aperture observation.

References. — (1) Jenniskens & Greenberg 1993; (2) Fitzpatrick & Massa 1990

TABLE 2  
ASURV RESULTS

$W_{\lambda}/E(B - V)$ versus	Spearman $\rho$	$t$ value <sup>a</sup>	probability <sup>b</sup>
$x_0$	0.236	1.83	0.072
$\gamma$	0.158	1.21	0.232
$c_1$	-0.369	-3.00	0.004
$c_2$	0.395	3.25	0.002
$c_3$	0.203	1.56	0.123
$c_4$	0.667	6.76	$8 \times 10^{-9}$

<sup>a</sup> $t = \rho \sqrt{\frac{N-2}{1-\rho^2}}$ , where  $N = 59$  is the number of data points.

<sup>b</sup>Probability that result is consistent with the null hypothesis.

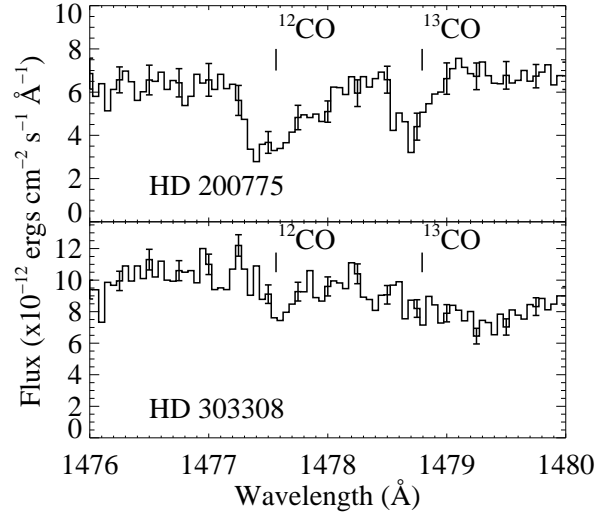


FIG. 1.— Sample spectra showing an example of a strong CO  $A - X$  (2-0) absorption (HD 200775) and weak (HD 303308). The rest wavelengths of the R(0) lines for the  $^{12}\text{CO}$  and  $^{13}\text{CO}$  are indicated.

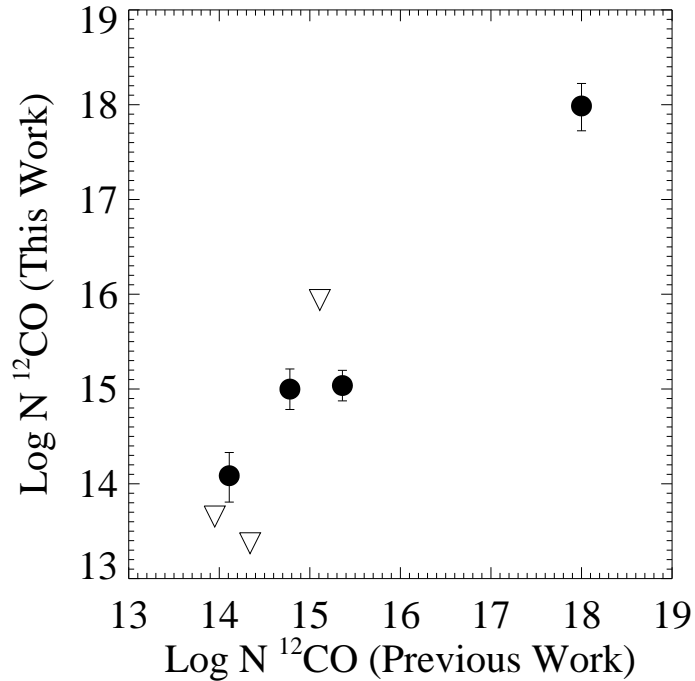


FIG. 2.— Log-log plot of  $^{12}\text{CO}$  column density in  $\text{cm}^{-2}$  comparing our data to that listed in Federman et al. (1994) for those sight lines in common. Column densities were determined using a curve-of-growth method assuming a doppler parameter  $b = 1 \text{ km s}^{-1}$  and rotational excitation temperature  $T = 4 \text{ K}$ . Upper limits ( $2\text{-}\sigma$ ) are shown as open triangles.

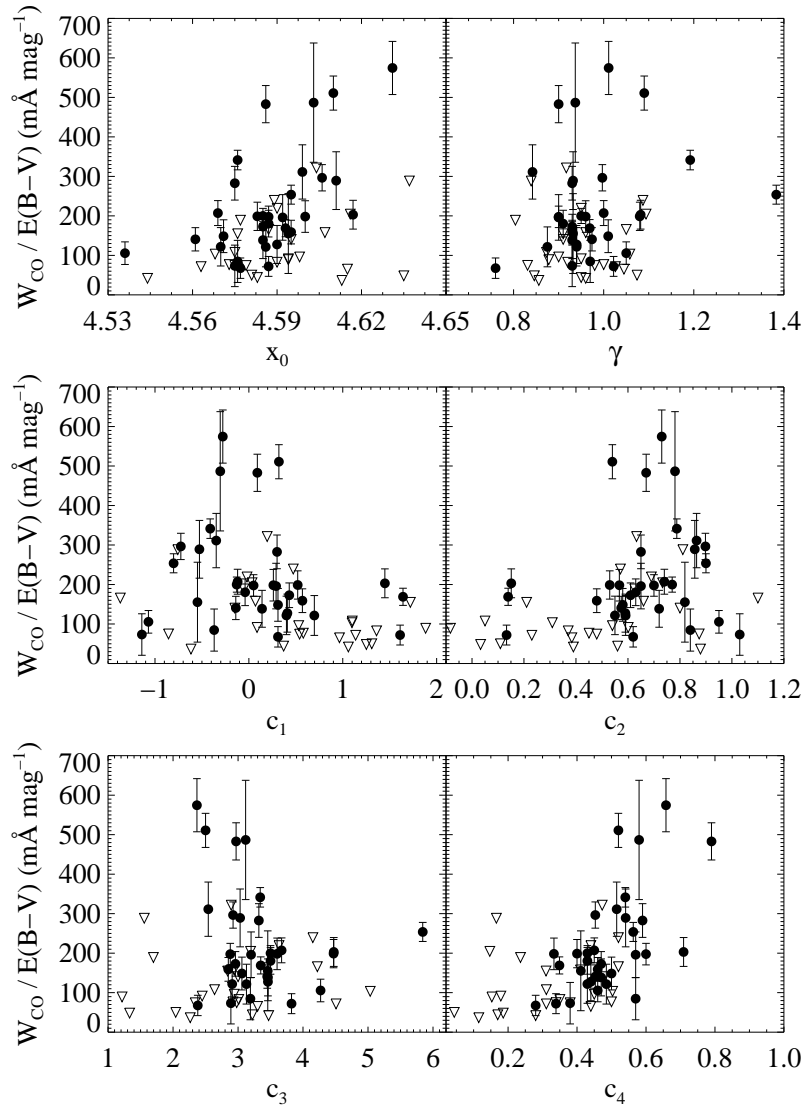


FIG. 3.— Correlation diagrams for the normalized equivalent width of the CO A – X (2–0) band in  $\text{m}\text{\AA}$  per magnitude of  $E(B - V)$ . Upper limits ( $2\sigma$ ) are shown as open triangles.



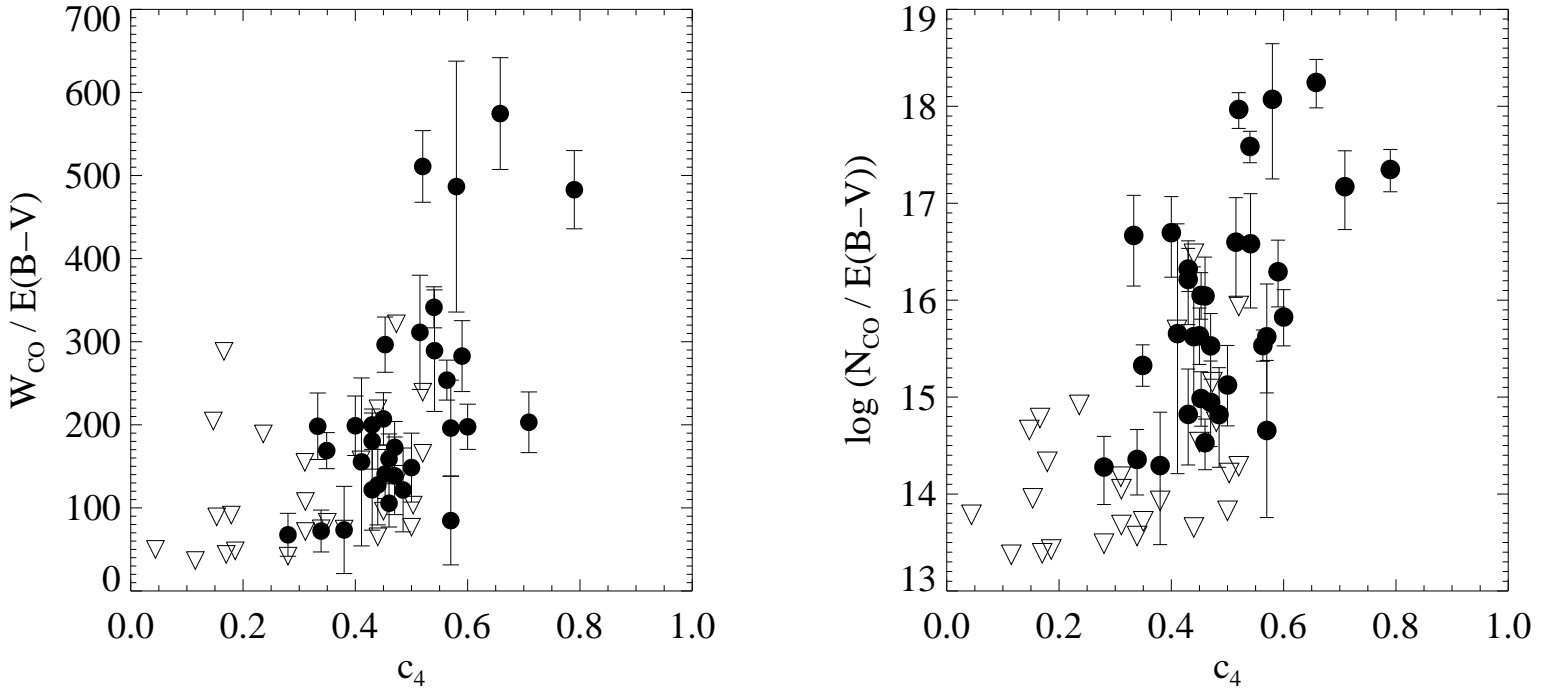


FIG. 4.— Left panel: Correlation diagram for the normalized equivalent width in  $\text{m}\text{\AA}$  per magnitude of  $E(B-V)$  versus  $c_4$ . Upper limits ( $2\text{-}\sigma$ ) are shown as open triangles. Right panel: Correlation diagram for column density in  $\text{cm}^{-2}$  per magnitude assuming  $T = 4\text{ K}$  and  $b = 1\text{ km s}^{-1}$ .

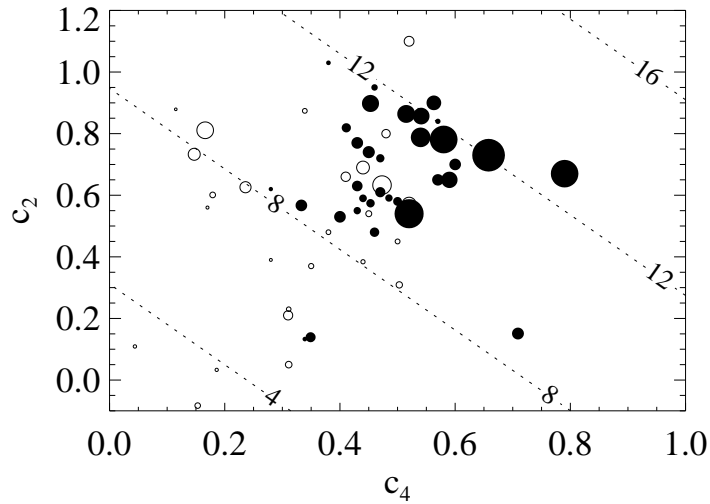


FIG. 5.— Plot of  $c_2$  v.  $c_4$ . The size of the circle indicates the strength of the CO absorption. Open circles are  $2\text{-}\sigma$  upper limits. The dotted lines correspond to constant  $k(x)$  for  $\lambda = 1076\text{ \AA}$ , with increasing extinction to the upper right.

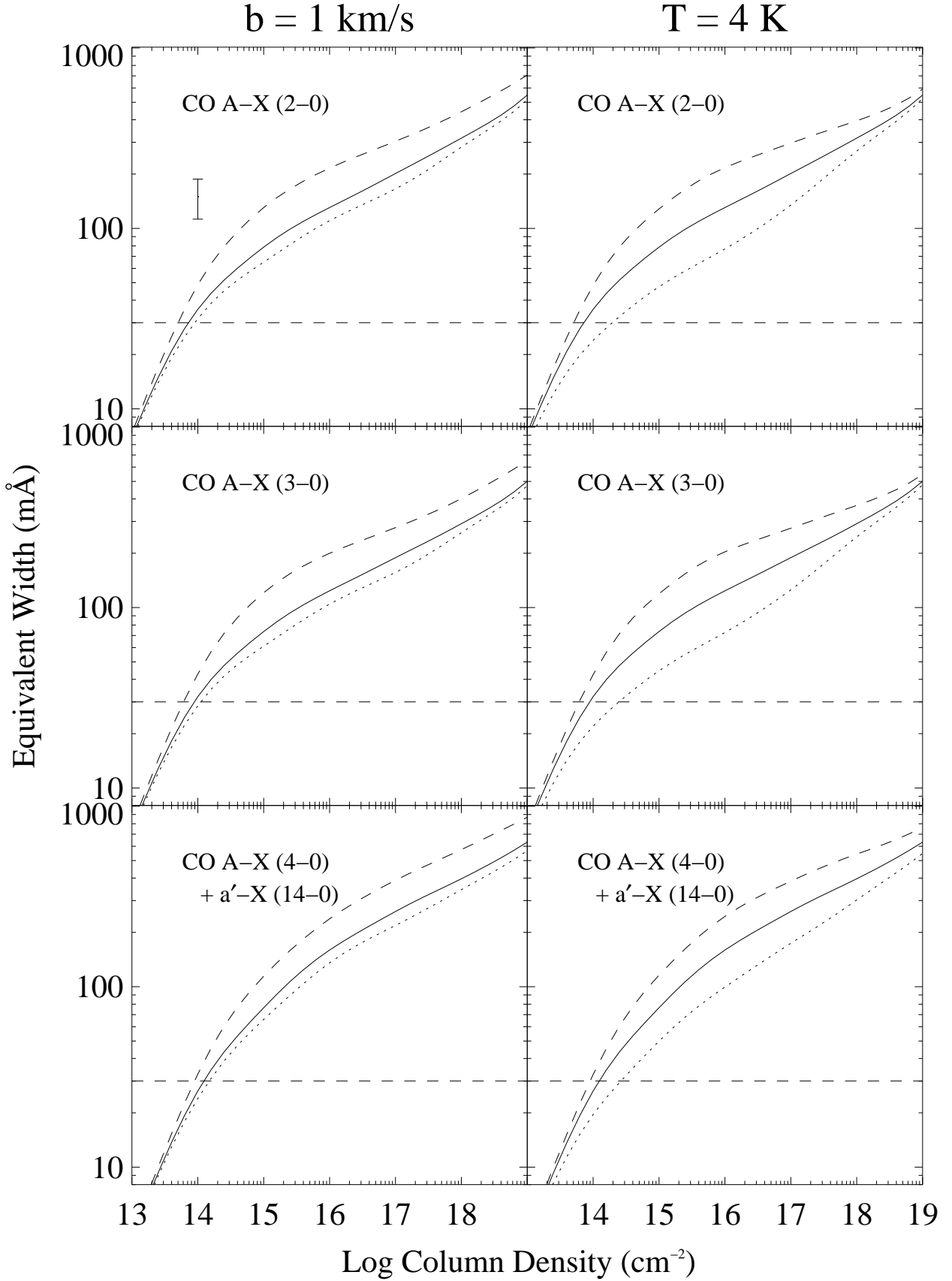


FIG. 6.— Curves-of-growth for the CO A-X (2-0), (3-0), and (4-0) bands. The (4-0) band is blended with the  $a'$ -X (14-0) band. The left panels are for  $b = 1 \text{ km s}^{-1}$  with dashed, solid and dotted lines corresponding to a rotational temperature of  $T = 10, 4,$  and  $3 \text{ K}$  respectively. The right panels are for  $T = 4 \text{ K}$  with dashed, solid and dotted lines corresponding to a doppler parameter  $b = 2, 1,$  and  $0.5 \text{ km s}^{-1}$  respectively. A horizontal dashed line shows our typical  $30 \text{ mÅ}$  detection limit. The top left panel shows a typical error bar in equivalent width.